Available online at www.sciencedirect.com
SCIENCE DIRECT
International Journal of Heat and Mass Transfer 49 (2006) 4013–4022
International Journal of HEAT and MASS TRANSFER
www.elsevier.com/locate/ijhmt

Shape optimization of three-dimensional channel roughened by angled ribs with RANS analysis of turbulent heat transfer

Hong-Min Kim, Kwang-Yong Kim *

Department of Mechanical Engineering, Inha University, 253 Yonghyun-Dong, Nam-Gu, Incheon 402-751, Republic of Korea

Received 4 April 2004; received in revised form 15 March 2006
Available online 9 June 2006

Abstract

A numerical procedure for optimizing the shape of three-dimensional channel with angled ribs extruded on both walls is presented to enhance turbulent heat transfer. The response surface based optimization is used as an optimization technique with Reynolds-averaged Navier–Stokes analysis of fluid flow and heat transfer. Shear stress transport (SST) turbulence model is used as a turbulence closure. Computational results for heat transfer rate show good agreements with experimental data. Four dimensionless variables such as, rib pitch-to-rib height ratio, rib height-to-channel height ratio, streamwise rib distance on opposite wall to rib height ratio, and the attack angle of the rib are chosen as design variables. The objective function is defined as a linear combination of heat transfer and friction loss related terms with a weighting factor. D-optimal method is used to determine the training points as a mean of design of experiment. Sensitivity of the objective function to each design variable has been evaluated. And, optimal values of the design variables have been obtained in a range of the weighting factor.

1. Introduction

With the increasing emphasis on energy savings, various heat transfer augmentation techniques such as pin fins, dimples, swirl chambers, and rib turbulators are developed and utilized in many industrial devices. Among them, attachment of ribs to flow passages becomes one of the widely used means of heat transfer augmentation technique, and has many industrial applications such as serpentine internal cooling passages in high temperature gas turbine blades, corrugated plate heat exchangers, and electronic cooling devices. Artificial ribs attached on the surface deduce secondary flows which have a vital role in heat transfer mechanism, increase the production of turbulent kinetic energy to activate small and large scale mixing, and generate coherent flow structure in the form of streamwise vortices. But, attached ribs also cause inevitable extra flow resistances, while augmenting heat transfer rate. Thus, to optimize the shape of rib-roughened surface, it is indispensable to compromise between enhancement of heat transfer and reduction of friction drag.

Many experimental works have been carried out to develop high-performance heat transfer surfaces roughened by square ribs for various heat exchanging devices. Rau et al. [1] performed aerodynamic and heat transfer measurements in a square channel with single surface roughened by ribs, being perpendicular to the main flow direction, to find the effect of rib pitch on the heat transfer rate. In the experimental work of Han et al. [2], the effects of the rib angle of attack and rib pitch-to-height ratio have been investigated on the pressure drop and the average heat transfer coefficients in the fully developed turbulent air flow in a square duct with two opposite rib-roughened walls. And, correlations for average friction factor and average heat transfer coefficient have been derived. Local heat transfer and friction loss in a square duct roughened by various types of continuous and discrete rib turbulators were examined by Cho et al. [3]. They recommended 90° in-lined array for high thermal performance. In addition

* Corresponding author. Tel.: +82 32 872 3096; fax: +82 32 868 1716.
E-mail address: kykim@inha.ac.kr (K.-Y. Kim).

0017-9310/$ - see front matter © 2006 Elsevier Ltd. All rights reserved.
doi:10.1016/j.ijheatmasstransfer.2006.03.039

Nomenclature

A	streamwise rib distance on opposite wall or area of heated surface
B	channel width
c_p	specific heat
D	channel height
D_h	channel hydraulic diameter
F	objective function
f	friction factor
H	rib height
k	fluid thermal conductivity
L	length of the channel
Nu	local Nusselt number
Nu_a	average Nusselt number
Pi	rib pitch
Pr	Prandtl number
p, Δp	pressure and pressure drop in a channel, respectively
$\hat{p}$	periodic component of pressure
q_0	wall heat flux
Re	Reynolds number ($= \overline{U}D_h/\nu$)
R^2_{adj}	adjusted R square
T	local mean temperature
T_w	wall temperature
$\hat{T}$	periodic component of temperature
U_i	mean velocity components ($i = 1, 2, 3$)
$\overline{U}$	averaged axial velocity
W	rib width
x, y, z	streamwise, spanwise, and cross-streamwise coordinates, respectively
x_j	coordinates ($j = 1, 2, 3$)

Greek symbols

α	angle of attack of the rib
β	weighting factor in objective function
γ	pressure gradient in streamwise direction
ν	kinematic viscosity
ρ	fluid density
σ	increasing rate of bulk temperature in axial direction

to the experimental works, many numerical researches [4–6] were performed to predict fluid flow and heat transfer in ribbed channels, but most of them were confined to compare the accuracy of the various turbulence models, not to find the optimal shape of the rib.

In many experimental and numerical works, the main purpose was to investigate the effect of the angle of attack and rib pitch-to-height ratio on the heat transfer coefficient and friction factor, and also to find the optimal case which gives the best thermal performance among a few tested cases. Thus, the optimal shape of rib-roughened channel, considering wide ranges of geometric variables, was not suggested. But, Kim and Kim [7] presented an investigation on a gradient-based numerical optimization technique coupled with Reynolds-averaged Navier–Stokes (RANS) analysis of turbulent flow and heat transfer for the design of rib-roughened surface in case of single surface roughened in two-dimensional channel. They suggested the optimal values of rib width-to-height ratio and rib pitch-to-height ratio with the objective function defined as linear function of heat transfer coefficient and friction drag coefficient, and showed that the numerical optimization method is a quite effective and reliable way of designing heat transfer surface.

Convective heat transfer of the surface roughened by square ribs is affected significantly by the flow properties, such as reattachment length of separated streamline and turbulence intensities, as well as Reynolds number. Therefore, shape optimization of rib-roughened surface for enhancement of turbulent heat transfer should be based on precise analysis of the flow structure. With the aid of high-performance computers, numerical optimization techniques based on Reynolds-averaged Navier–Stokes analysis have been developed rapidly for the last decade. Among the methods of numerical optimization, response surface based optimization method [8], as a global optimization method, has many advantages over the gradient-based methods [7,9]. Recently, the response surface based optimizations are being applied to many single- and multi-disciplinary optimization problems [10–12].

In this work, a numerical optimization procedure is presented for the design of heat transfer surface roughened by square ribs in a three-dimensional channel with both surfaces roughened. Turbulent convective heat transfer is analyzed with Reynolds-averaged Navier–Stokes analysis. Response surface method is employed to maximize thermal performance of the surface with four design variables, i.e., rib pitch-to-rib height ratio, rib height-to-channel height ratio, streamwise rib distance on opposite wall to rib height ratio, and the attack angle of the rib.

2. Numerical analysis

For the analysis of complex fluid flow and convective heat transfer in a rib-roughened three-dimensional channel, CFX-5.6 [13] which employs unstructured grids was used in this work.

To adopt periodic boundary conditions, modifications of source terms in streamwise momentum and energy equations have been made to calibrate the gradual decrease and increase of pressure and temperature, respectively. Finally, for three-dimensional steady incompressible flows, mass, momentum, and energy conservation equations in tensor form can be written as follows:

$$\frac{\partial U_i}{\partial x_i} = 0 \tag{1}$$

$$U_j \frac{\partial U_i}{\partial x_j} = \frac{\partial}{\partial x_j}\left[\nu \frac{\partial U_i}{\partial x_j}\right] - \frac{1}{\rho}\frac{\partial \hat{p}}{\partial x_i} + \gamma \delta_{1i} \tag{2}$$

$$\frac{\partial}{\partial x_j}\left(\rho c_p U_j \widehat{T}\right) = \frac{\partial}{\partial x_j}\left[k \frac{\partial \widehat{T}}{\partial x_j}\right] - \sigma U_j \delta_{1j} \tag{3}$$

where $\hat{p}(x,y,z)$ and $\widehat{T}(x,y,z)$ are the pressure and temperature transformed as follows in order to use the periodic boundary conditions [14] in streamwise direction, x.

$$\hat{p}(x,y,z) = p(x,y,z) + \gamma x \tag{4}$$

$$\widehat{T}(x,y,z) = T(x,y,z) - \sigma x \tag{5}$$

Here, γ is the pressure gradient along the streamwise direction, and σ is the rate of bulk temperature increase due to wall heat flux, q_0:

$$\sigma = \frac{2q_0}{\overline{U}D} \tag{6}$$

Shear stress transport (SST) turbulence model with automatic wall treatment [15] is used as a turbulence closure. Basically, SST model combines the advantages of the k–ε and k–ω models with a blending function. The k–ω model is activated in the near-wall region, and the k–ε model is used in the rest region. Bardina et al. [16] showed that the SST model captures separation under adverse pressure gradient well compared to other eddy viscosity models, and, thus, predicts well the near-wall turbulence that plays a vital role to the accurate prediction of the turbulent heat transfer. Numerical model of Lai and So [17] is adopted for modeling of turbulent heat flux.

Geometric parameters and computational domain are shown in Fig. 1, where the attack angle, 90° implies the flow normal to the ribs. Computational domain is composed of one pitch of rib displacement to reflect periodic behavior of flow fields. Therefore, many fragments of ribs are included in the computational domain, especially for the small angle of attack of the rib. In Fig. 2, two examples of the grid system are shown for whole computational domain and around the rib. Unstructured tetrahedral grid system is used with the hexahedral at the wall region to resolve high velocity gradient. First grid points are placed at $0.0002D$ from the walls to satisfy $y+$ less than 1.0. In some cases, for example, with small attack angle as shown in Fig. 2(b), it was very difficult to get a converged solution due to multiple flow separations on the periodic boundaries. In that case, careful adjustment of grid system was needed to guarantee the convergence of numerical solution.

In the present calculation, uniform heat flux is specified on the rib surfaces and channel walls between ribs. Bulk velocity corresponding to Reynolds number, 30,000, and constant temperature are set at all computational nodes as initial values to help the faster convergence of the iterative calculation.

With the periodic conditions, it is difficult to assign specific flow rate to the calculated flow. Thus, the iterative procedure is inevitably employed. At the initial stage of the calculation, pressure gradient in streamwise direction is assumed through the source term in the streamwise momentum equation, and is continually updated until Reynolds number reaches within 1% of target Reynolds number.

3. Optimization techniques

Recently, as a global optimization method, polynomial based response surface method (RSM) [8] which terms the collective use of design of experiment (DOE) techniques, regression analysis, and analysis of variance

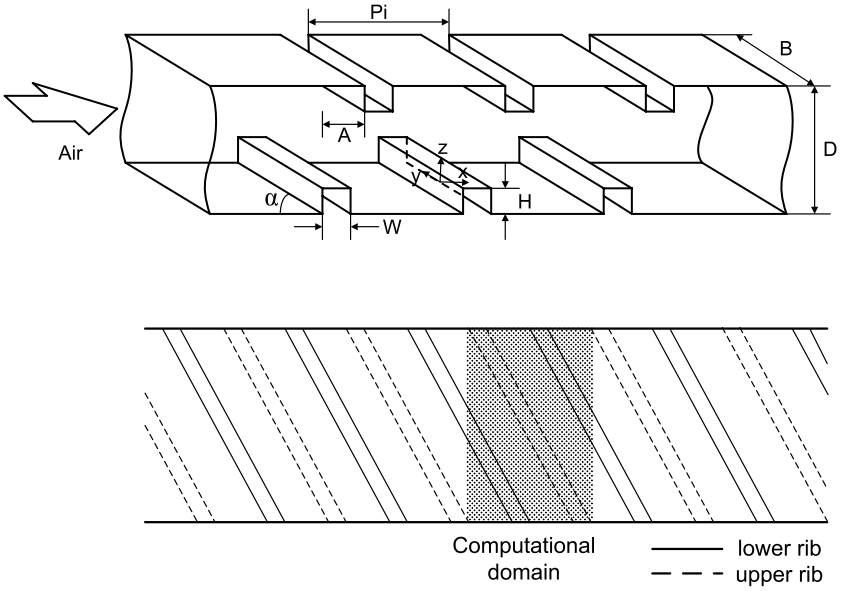

Fig. 1. Geometric parameters and computational domain.

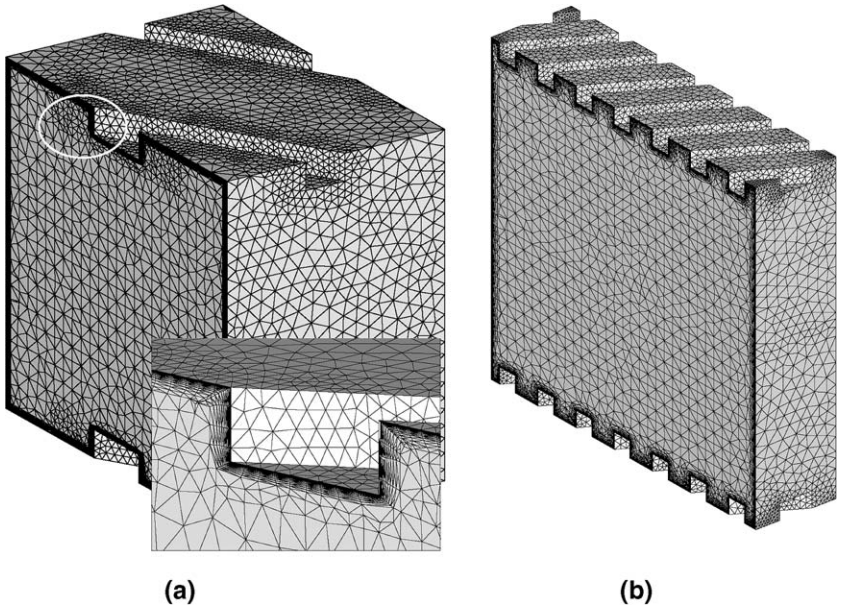

Fig. 2. Examples of grid system: (a) $Pi/H = 8.0$ and $\alpha = 60°$, (b) $Pi/H = 5.0$ and $\alpha = 30°$.

(ANOVA), is widely used, instead of old-fashioned gradient-based optimization methods.

In the present work, RSM was used to obtain an optimal shape of the rib-roughened three-dimensional channel. The optimization problem is defined as minimization of an objective function, $F(\mathbf{x})$ with $x_i^{\mathrm{l}} \leqslant x_i \leqslant x_i^{\mathrm{u}}$, where $\mathbf{x}$ is a vector of design variables, and x_i^{l} and x_i^{u} are lower and upper bounds of each design variable, respectively. RSM performs a series of numerical analyses, for a prescribed set of design points, and to construct a response surface using the calculated quantities over the design space.

A second-order polynomial has been used to represent response surface, and coefficients of the polynomial have been determined by the least square method. Prescribed set of design points, so-called training points, was selected by D-optimal experimental designs [8]. Appealing properties of D-optimal experimental designs [18] are to minimize the uncertainty in the estimated coefficients and to minimize the maximum variance of any predicted value by choosing the training points to maximize $|\mathbf{x}^{\mathrm{T}}\mathbf{x}|$. And also, it is known as a useful and reliable way of constructing response surface with a small number of design points which is only 1.5–2.5 times the number of polynomial coefficients. Unal et al. [19] showed that D-optimal design provides an efficient approach for building the response surface model and implementing multi-disciplinary optimization.

The three-dimensional channel with angled-rib-roughened surfaces is shown in Fig. 1. With seven geometric parameters, i.e., height of the channel (D), width of the channel (B), height of the rib (H), width of the rib (W), rib pitch (Pi), streamwise rib displacement on opposite wall (A), and the angle of attack of the rib (α), there exist six dimensionless variables; H/D, B/D, W/H, Pi/H, A/H, and α. In the present optimization, W/H and B/D were identically set to be 1.0 to reduce the number of design variables. B/D is usually restricted by the allowable space where rib turbulators are placed. And, according to the authors' previous work [20], the effects of W/H on heat transfer and friction loss are much smaller than those of the angle of attack. Therefore, four design variables such as H/D, Pi/H, A/H, and α were selected as design variables in the optimization.

To maximize the performance of the ribs, the optimal shape should be determined by compromising between the enhancement of heat transfer and reduction of friction loss. After the definition proposed by Gee and Webb [21], average Nusselt number and 1/3 power of friction factor became indexes of representing the thermal performance of ribbed channel, as used in many experimental works [2,3,22], and in the present optimization, those two objectives are combined with weighting factor which is frequently adopted in multi-objective optimizations. Therefore, the present optimization problem is defined as minimization of following objective function:

$$F = F_{Nu} + \beta F_{\mathrm{f}} \tag{7}$$

where β is a weighting factor. This factor should be determined by the designer considering energy economy of the whole system. The first term on the right-hand side is defined as an inverse of average Nusselt number:

$$F_{Nu} = \frac{1}{Nu_{\mathrm{a}}} \tag{8}$$

where

$$Nu_{\mathrm{a}} = \frac{\int_A \frac{Nu}{Nu_{\mathrm{s}}}\,\mathrm{d}A}{A}$$

$$Nu = \frac{q_0 D_{\mathrm{h}}}{k(T_{\mathrm{w}} - T)}$$

$$Nu_{\mathrm{s}} = 0.023 Re^{0.8} Pr^{0.4}$$

Nu is the local Nusselt number, and Nu_s is the Nusselt number obtained from the Dittus–Boelter correlation, which is for the fully developed turbulent flows in a smooth pipe, and the integration is performed over the heated surface (A) between the ribs.

The second term which is related to friction loss is defined as follows:

$$F_f = \left(\frac{f}{f_0}\right)^{1/3} \tag{9}$$

where

$$f = \frac{\Delta p D_h}{2\rho \overline{U}^2 L}$$

$$f_0 = 2(2.236 \ln Re - 4.639)^{-2}$$

f_0 is a friction factor for fully developed flow in a smooth pipe, and is obtained from Petukhov empirical correlation [23] which is modified from the Karman–Nikuradse correlation for the best fit in the range, $10^4 < Re < 10^6$.

4. Results and discussion

To find optimal number of grids, five different numbers were tested for both surfaces roughened channel with the conditions same as the experiment by Cho et al. [3], as shown in Fig. 3. As the number of grids increases, the error compared to the results with the finest grids (1.1×10^5) decreases monotonically as the sequence of 8.4%, 4.0%, 1.9%, and 1.0%. Therefore, from the results, the number of grids, 1.0×10^5 is selected as an optimal one.

For the validation of present numerical solution, the results for the distribution of local Nusselt number along the bottom centerline between the ribs are compared with the experimental data of Rau et al. [1] at Reynolds number, 30,000 with $B/D = 1.0$, $H/D = 0.1$, $Pi/H = 9.0$, $A/H = 0.0$, and $\alpha = 90°$, in Fig. 4. In this figure, the maximum value of local Nusselt number on the surface between the ribs is underestimated, but general trend of the distribution is acceptable in comparison with the experimental data. This prediction, however, looks better than those of Ooi et al. [6], who also calculated the local Nusselt number with single surface roughened by perpendicular ribs by using v2f turbulence model. The discrepancy in the local Nusselt number distribution, not in the average level, is expected not to have a large influence on the optimization results. In Fig. 5, computed average Nusselt numbers with different attack angles for the same condition as the experiment by Han et al. [2] for $Pi/H = 20.0$, are compared with the experimental data of Han et al. [2] for $Pi/H = 10.0$ and 20.0, $A/H = 0.0$ and $H/D = 0.063$, and Cho et al. [3] for $Pi/H = 8.0$, $A/H = 0.0$, and $H/D = 0.08$. The computational Nusselt numbers are in good agreements with corresponding experimental data. Computational results for friction factor are also validated by comparing with the experimental data of Han et al. [2] for $Pi/H = 20.0$ as shown in Fig. 6. The agreements

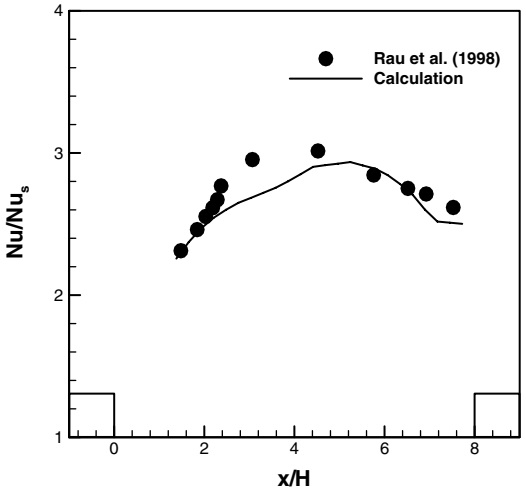

Fig. 4. Validation of computed local Nusselt number for $\alpha = 90°$ along the bottom centerline.

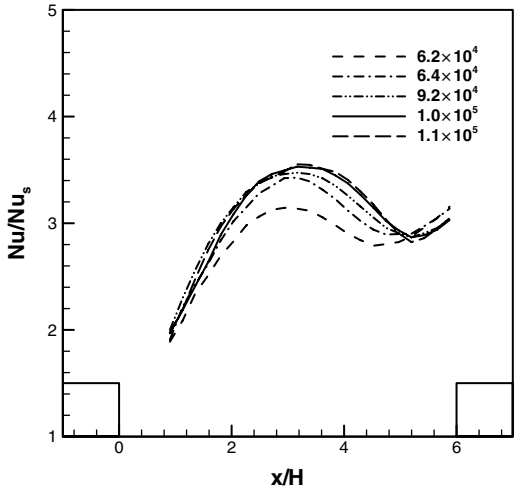

Fig. 3. Grid dependency test.

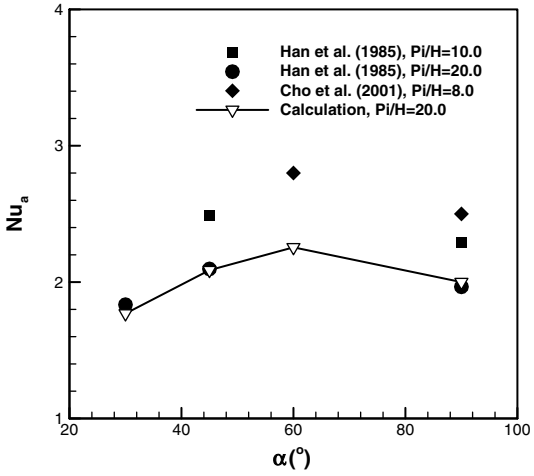

Fig. 5. Validation of computed average Nusselt number.

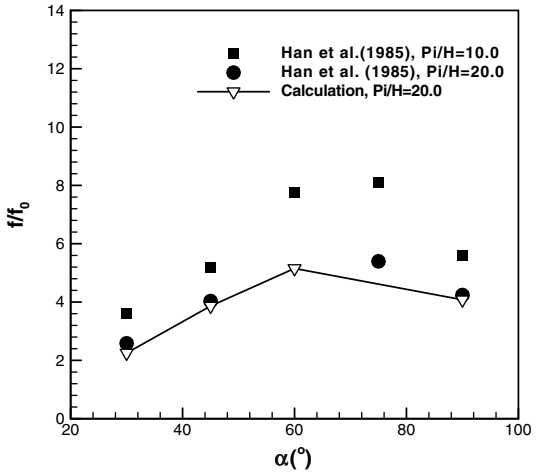

Fig. 6. Validation of computed friction factor.

with experimental data are generally satisfactory enough to support the validity of the results.

In the present optimization, Reynolds number based on hydraulic diameter with 25 °C air is 30,000, and uniform heat flux is imposed on both walls. For the optimization, response surface based optimization is used and 27 training points are selected by D-optimal experimental designs to construct the response surface. Ranges of design variables are listed in Table 1. Lower and upper limits of Pi/H are selected as 5.0 and 20.0, respectively, because maximum heat transfer rates were obtained within this range in many experimental works [1,4,24] and in numerical work of Habib et al. [25]. Design variable for asymmetry of the ribs, A/H ranges from 0.0 to 2.5 that correspond to symmetric and staggered arrangements of the ribs, respectively. For H/D, its design space is set from 0.05 to 0.25. Below the lower limit, computational difficulty arose and, moreover, it is not compatible with the actual usage of general heat exchanger. And, over the upper limit, pressure drop increases abruptly as was indicated by Lopez et al. [26]. Lower and upper limits of α are selected as 30° and 90°, respectively, because maximum heat transfer rates were observed within this range in the experimental works of Han et al. [2] and Cho et al. [3], and also in the computational work of Tatsumi et al. [27].

Numerical optimizations have been performed in the range from 0.0 to 0.1 of the weighting factor. To measure the uncertainty in the set of coefficients in a polynomial, analysis of variance and regression analysis provided by t-statistic [8] are implemented. For example, R^2_{adj} for $\beta = 0.02$ is 0.959 as shown in Table 2. Guinta [28] suggested that the typical values of R^2_{adj} are in the range, $0.9 \leqslant R^2_{adj} \leqslant 1.0$, when the observed response values are accurately predicted by the response surface model. In this respect, the present response surfaces are quite reliable since R^2_{adj} is over 0.93 for all cases of optimization.

Figs. 7 and 8 show results of sensitivity analyses for two components of the objective function. Here, the percent change of each design variable, dv is varied within ±10% of the optimal value, and the subscript, opt represents the value at optimal shape with $\beta = 0.05$. From these sensitive analyses, it is evident that heat transfer and friction coefficients are more sensitive to rib height and the angle of attack of the rib than to rib pitch and asymmetry of the ribs near the optimal point. The sensitivity to angle of attack is almost same as that to rib height in case of heat transfer related term, but is quite lower than that to rib height in case of friction loss term. The results of sensitivity analysis for the objective function with $\beta = 0.05$ are shown in Fig. 9. It is found that the objective function is most sensitive to the rib height as expected from Figs. 7 and 8. Fig. 8 shows that friction loss related component of the objective function is far from the minimum at the optimum shape, unlike the case of heat transfer related term shown in Fig. 7.

Results of optimization for $\beta = 0.02$ are shown in Table 3. The reference shape was chosen arbitrary among the cases with $\alpha = 60°$, and the perpendicular shape indicates the shape with $\alpha = 90°$. The optimal shape gives average Nusselt number 3.96% and 43.4% larger than those of the reference and the perpendicular shapes, respectively. But, the value of friction loss related term (F_f) in optimal

Table 1
Design variables and ranges

Design variable	Lower bound	Upper bound
H/D	0.05	0.25
Pi/H	5.0	20.0
A/H	0.0	2.5
α	30.0°	90.0°

Table 2
Results of ANOVA and regression analysis

β	R	R^2	R^2_{adj}
0.02	0.989	0.983	0.959

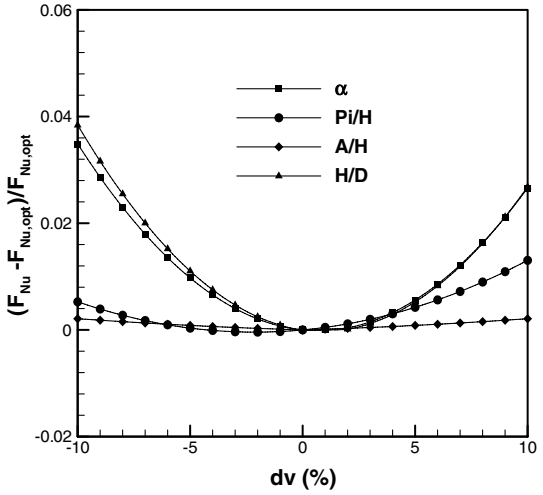

Fig. 7. Sensitivity analysis of F_{Nu} for optimal shape ($\beta = 0.05$).

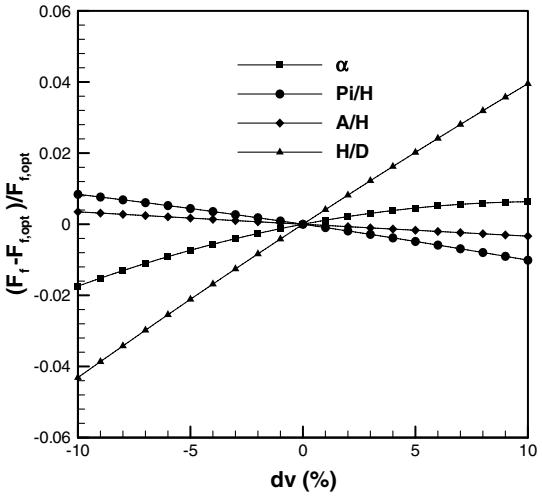

Fig. 8. Sensitivity analysis of F_f for optimal shape ($\beta = 0.05$).

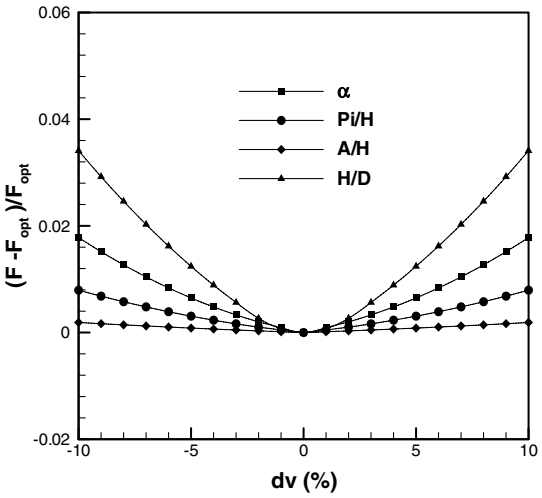

Fig. 9. Sensitivity analysis of objective function for optimal shape ($\beta = 0.05$).

Table 3
Results of optimization for $\beta = 0.02$

	Design variable				Nu_a	F_f	Objective function
	H/D	Pi/H	A/H	α			
Perpendicular shape	0.21	12.7	0.70	90.0°	1.9533	2.3265	0.55848
Reference shape	0.25	12.5	1.25	60.0°	2.6946	2.8464	0.42804
Optimal shape	0.21	12.7	0.70	55.4°	2.8013	2.7381	0.41174

case is 17.7% larger than that of the perpendicular shape. This is not surprising when we recall the experimental results of Han et al. [2], where friction factor of optimal rib is much larger than that of perpendicular rib. Finally, the objective function is reduced to 3.81% and 26.3% of the value of reference shape and perpendicular shape, respectively.

Local Nusselt number contours on both walls between ribs are shown in Fig. 10 for three types of rib arrangement, i.e., perpendicular, reference, and optimal shapes. In all cases, heat transfer rate decreases abruptly just behind the rib due to flow separation, and increases downstream to reach the maximum near the reattachment line. Then, it shows another peak before the next rib due to the collision of fluid lumps to the front of the next rib. It is noted that heat transfer rate on bottom wall is found to be higher than that on top wall around the reattachment lines, since the flow accelerated passing through the relatively narrow passage between bottom and top ribs reattaches on the bottom wall first, and has second reattachment with deceleration on the top wall. And, the optimum shape gives the higher heat transfer rate and the shorter reattachment length downstream of the rib due to the relatively smaller gap between bottom and top ribs compared with the reference shape. From these results, it is found that length of the separation region plays a vital role in enhancing the heat transfer rate. In other words, the smaller separation region gives the better heat transfer rate. The smallest region of separation is found in the optimal shape of the ribbed channel compared to the other two cases. As a result, heat transfer is augmented in a wide region of the surface between the ribs.

Fig. 11 shows streamlines on three different y–z planes in optimal channel. The abscissa and the ordinate in these figures are same as indicated in Fig. 1. It is noted that three separate vortices are formed just after the rib. But, three vortices in Fig. 11(a) and (b) are not identical. The two vortices depicted at the bottom half of Fig. 11(a) merge to one which is shown at the bottom in Fig. 11(b), and a new vortex is generated at the upper half in Fig. 11(b). And, the two vortices which occupy upper region in Fig. 11(b) are combined into one at $x/H = 7.0$ (Fig. 11(c)).

The spanwise mixing induced by these vortices gives rise to large heat transfer augmentation even far downstream of the rib. In Fig. 12, local Nusselt number distributions along the center line, $y/B = 0$, are compared for three shapes. The maximum overall heat transfer occurs at optimal shape which gives the shortest length of flow reattachment, where the local heat transfer rate reaches the maximum.

Optimal values of four design variables are plotted for different weighting factors in Figs. 13 and 14. With the increase of the weighting factor, in other word, as designer's purpose is shifted to the reduction of pressure drop, rib pitch and rib displacement on opposite wall increase, but the angle of attack and rib height decrease. As rib pitch increases, pressure recovery after the separation also increases, and hence optimal value of Pi/H moves toward the larger value with increasing weighting factor. As for rib displacement on opposite wall, it is interesting to notice that when only the heat transfer performance is the matter of concern, still an asymmetric rib arrangement shows the best performance than a symmetric case. It is difficult to discuss on this result because no experimental

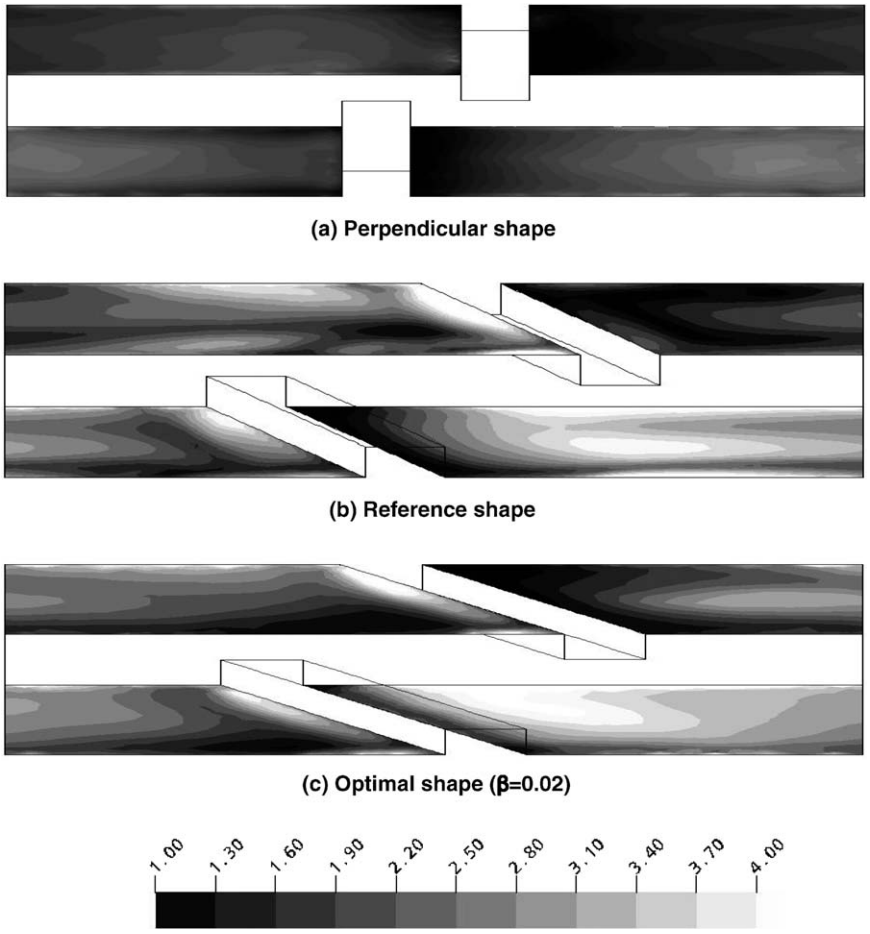

Fig. 10. Normalized local Nusselt number contours.

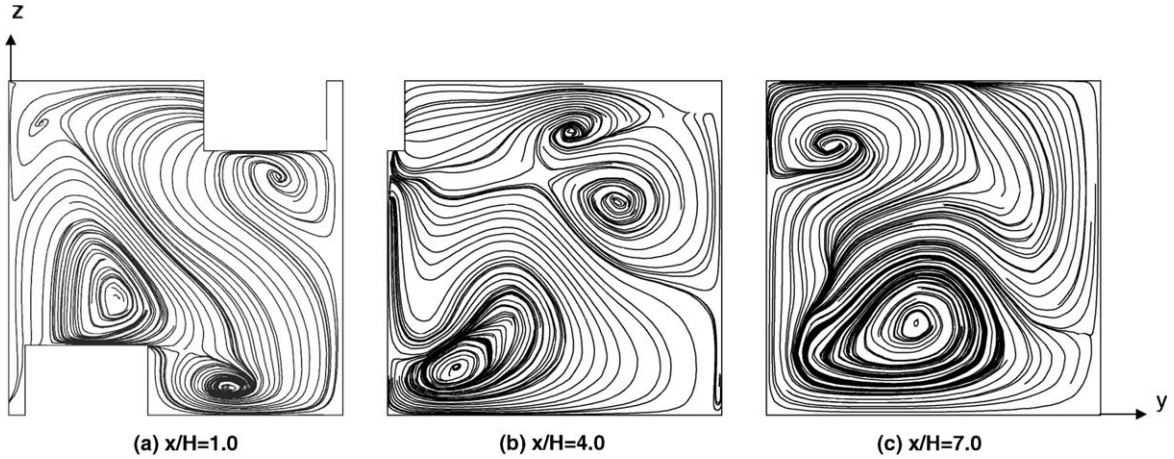

Fig. 11. Streamlines on y–z planes in optimal channel ($\beta = 0.02$).

work has been performed for this case. But, it is thought that flow interference by an asymmetric placement of upper and lower ribs increases turbulent intensity close to wall and plays a vital role to enhance heat transfer augmentation. Actually, turbulent kinetic energy adjacent to the wall of asymmetric placement is 5–40% larger than that of symmetric ones among the calculated cases.

Tiggelbeck et al. [29] reported that, for a wing vortex generator, the longitudinal flow structure which produces effective heat transfer augmentation at the wall over large span of streamwise distance is not clearly formed for the angle of attack larger than 70°. And, Tatsumi et al. [27] reported, from their numerical work for an oblique discrete rib, that maximum heat transfer rate is observed at the

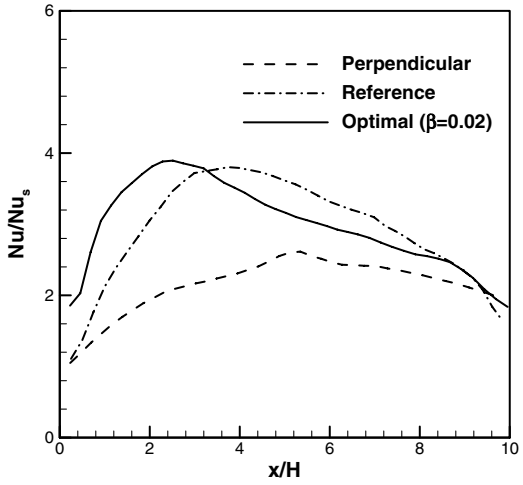

Fig. 12. Local Nusselt number distributions between ribs on bottom wall.

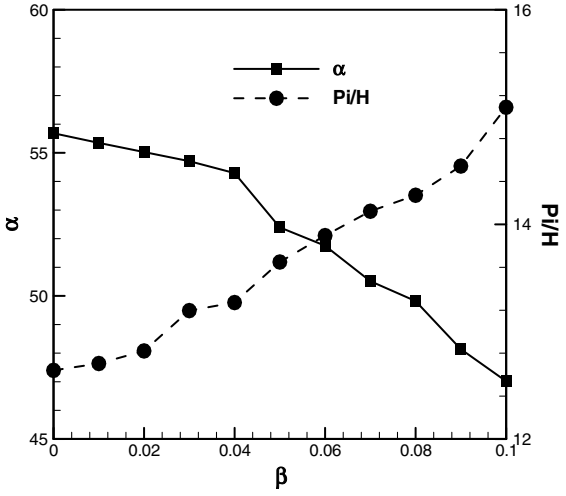

Fig. 13. Variations of optimal values of α and Pi/H.

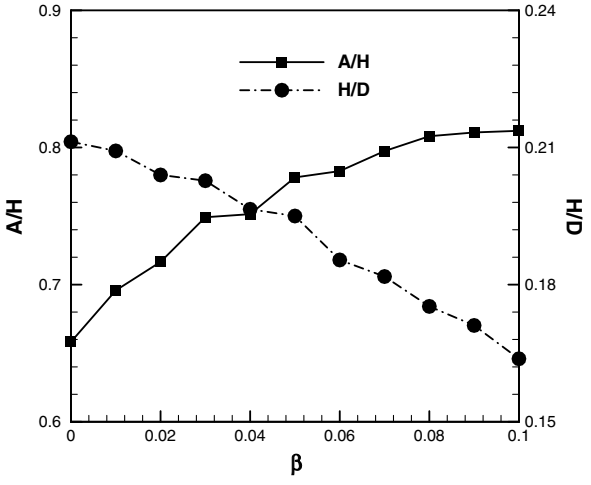

Fig. 14. Variations of optimal values of A/H and H/D.

angle of attack of 45° while maximum friction loss occurs at the angle of attack of 60°, and that a longitudinal vortex of large scale was found at the angle of attack less than 60°. From these previous results, it is estimated that optimal values exist between 45° and 60° of the angle of attack. And, it is found that the present optimization results, shown in Fig. 13, are consistent with these results.

The computations were carried out by personal computer with Intel Pentium IV CPU 2.4 GHz. The computing time of single flow analysis using CFX-5.6 is in the range of 7–20 h according to the geometry considered and the convergence rate.

5. Conclusions

Geometric shape of three-dimensional channel with both surfaces roughened by square ribs has been optimized to maximize the performance of heat transfer by response surface based optimization method coupled with Reynolds-averaged Navier–Stokes analyses of fluid flow and heat transfer. Calculated local and averaged Nusselt number distributions showed a reasonable agreement with experimental data, enough to be used in the optimization process. The objective function was defined in order to maximize the performance of the ribs by compromising between augmentation of heat transfer and reduction of friction loss with a weighting factor. Twenty-seven training points selected by D-optimal design of experiment for four design variables construct a reliable response surface. It is found that both of heat transfer and friction loss related components of objective function are most sensitive to the height of rib among the design variables. The optimal values of design variables were obtained with the variation of the weighting factor. As the weighting factor increases, in other word, as design emphasis is shifted to reduction of friction loss, optimal values of rib pitch-to-rib height ratio and rib displacement-to-rib height ratio increase, but those of attack angle and rib height-to-channel height ratio decrease.

Acknowledgment

This work was supported by Grant No. R01-2006-000-10039-0 from the Basic Research Program of the Korea Science and Engineering Foundation.

References

[1] G. Rau, M. Cakan, D. Moeller, T. Arts, The effect of periodic ribs on the local aerodynamic and heat transfer performance of a straight cooling channel, J. Turbomach. 120 (1988) 368–375.
[2] J.C. Han, J.S. Park, C.K. Lei, Heat transfer enhancement in channels with turbulence promoters, J. Eng. Turbines Power 107 (1985) 628–635.
[3] H.H. Cho, S.Y. Lee, S.J. Wu, The combined effects of rib arrangements and discrete ribs on local heat/mass transfer in a square duct, ASME 2001-GT-0175, 2001.
[4] R. Jia, B. Sunden, Prediction of turbulent heat transfer and fluid flow in 2d channels roughened by square and deformed ribs, ASME GT-2003-38226, 2003.
[5] H. Iacovides, M. Raisee, Recent progress in the computation of flow and heat transfer in internal cooling passages of turbine blades, Int. J. Heat Fluid flow 20 (1999) 320–328.

[6] A. Ooi, G. Iaccarino, P.A. Durbin, M. Behnia, Reynolds averaged simulation of flow and heat transfer in ribbed ducts, Int. J. Heat Fluid flow 23 (2002) 750–757.
[7] K.Y. Kim, S.S. Kim, Shape optimization of rib-roughened surface to enhance turbulent heat transfer, Int. J. Heat Mass Transfer 45 (2002) 2719–2727.
[8] R.H. Myers, D.C. Montgomery, Response Surface Methodology: Process and Product Optimization Using Designed Experiments, John Wiley & Sons, New York, 1995.
[9] S.Y. Lee, K.Y. Kim, Design optimization of axial flow compressor blades with three-dimensional Navier–Stokes solver, KSME Int. J. 14 (2000) 1005–1012.
[10] C.S. Ahn, K.Y. Kim, Aerodynamic design optimization of a compressor rotor with Navier–Stokes analysis, Proc. Inst. Mech. Eng., Part A – J. Power Energy 217 (2003) 179–184.
[11] J. Sobieszczanski-Sobieski, R.T. Haftka, Multi disciplinary aerospace design optimization: survey of recent development, AIAA 96-0711, 1996.
[12] W. Shyy, N. Papila, R. Vaidyanathan, K. Tucker, Global design optimization aerodynamics and rocket propulsion components, Prog. Aerospace Sci. 37 (2001) 59–118.
[13] CFX-5.6 Solver Theory, Ansys Inc., 2003.
[14] B.W. Webb, S. Ramadhyani, Conjugate heat transfer in a channel with staggered ribs, Int. J. Heat Mass Transfer 28 (1985) 1679–1687.
[15] F. Menter, T. Esch, Elements of industrial heat transfer predictions, in: 16th Bazilian Congress of Mechanical Engineering (COBEM), Uberlandia, Brazil, 2001.
[16] J.E. Bardina, P.G. Huang, T. Coakley, Turbulence modeling validation, AIAA Paper 97-2121, 1997.
[17] Y.G. Lai, R.M.C. So, Near-wall modeling of turbulent heat fluxes, Int. J. Heat Mass Transfer 33 (1990) 1429–1440.
[18] M.J. Box, N.R. Draper, Factorial designs, the $|X^{T}X|$ criterion, and some related matters, Technometrics 13 (1971) 731–742.
[19] R. Unal, R.A. Lepsch, M.L. McMillin, Response surface model building and multidisciplinary optimization using D-optimal designs, in: Seventh AIAA/USAF/NASA/ISSMO Symposium on Multidisciplinary Analysis and Optimization, 98-4759, 1998.
[20] H.M. Kim, K.Y. Kim, Optimization of the three-dimensional angled ribs with RANS analysis of turbulent heat transfer, ASME GT-2004-53346, 2004.
[21] D.L. Gee, R.L. Webb, Forced convection heat transfer in helically rib-roughened tubes, Int. J. Heat Mass Transfer 23 (1980) 1127–1136.
[22] M.E. Taslim, C.M. Wadsworth, An experimental investigation of the rib surface-averaged heat transfer coefficient in a rib roughened square passage, J. Turbomach. 119 (1997) 381–389.
[23] B.S. Petukhov, Advances in Heat Transfer, vol. 6, Academic Press, New York, 1970, pp. 503–504.
[24] F.P. Berger, K.-F.F.-L. Hau, Local mass/heat transfer distribution on surface roughened with small square ribs, Int. J. Heat Mass Transfer 22 (1979) 1645–1656.
[25] M.A. Habib, A.E. Attya, D.M. McEligot, Calculation of turbulent flow and heat transfer in channels with streamwise-periodic flow, J. Turbomach. 110 (1988) 405–411.
[26] J.R. Lopez, N.K. Anand, L.S. Fletcher, Heat transfer in a three-dimensional channel with baffles, Numer. Heat Transfer Part A 30 (1996) 189–205.
[27] K. Tatsumi, H. Iwai, K. Inaoka, K. Suzuki, Numerical analysis for heat transfer characteristics of an oblique discrete rib mounted in a square duct, Numer. Heat Transfer Part A 44 (2003) 811–831.
[28] A.A. Guinta, Aircraft Multi-disciplinary Design Optimization Using Design of Experimental Theory and Response Surface Modeling Methods, Ph.D. Dissertation, Department of Aerospace Engineering, Virginia, 1997.
[29] S. Tiggelbeck, N.K. Mitra, M. Fiebig, Flow structure and heat transfer in a channel with multiple longitudinal vortex generators, in: Proc. 2nd World Conf. on Experimental Heat Transfer, Fluid Mechanics and Thermodynamics, Dubrovnik, 1991, pp. 126–133.